Review

Porous Catalytic Membranes for CO_2 Conversion

Yi Guo[a], Cheng Qian[a], Yinglong Wu[a], Jiawei Liu[a], Xiaodong Zhang[a], Dongdong Wang[a], Yanli Zhao[a,b]*

[a] Division of Chemistry and Biological Chemistry, School of Physical and Mathematical Sciences, Nanyang Technological University, 21 Nanyang Link, 637371, Singapore

[b] School of Chemical and Biomedical Engineering, Nanyang Technological University, 62 Nanyang Drive, Singapore 637459, Singapore

*Corresponding author.

E-mail address: zhaoyanli@ntu.edu.sg (Y. L. Zhao)

ABSTRACT

Catalytic CO_2 conversion has witnessed a dynamic growth in recent decades. Various materials have been applied to reduce CO_2 into fuels and value-added chemicals. Normally, the powder-based catalysts cannot be directly utilized for CO_2 conversion. Much attention was paid to the study of catalytic membranes in order to overcome this issue, since it is convenient for catalytic membranes to be employed in devices for practical applications. In this review, the recent research development of porous catalytic membranes for CO_2 conversion is summarized. The preparations of representative porous catalytic membranes and

their CO_2 conversion methods, including electrocatalysis, photocatalysis, photoelectrocatalysis, thermalcatalysis and biocatalysis, are discussed in detail. This review is expected to provide deep understanding on the utilization of porous catalytic membranes for CO_2 conversion.
Keywords: Catalysis, Electrodes, CO_2 conversion, Membrane preparation, Porous membranes, Sustainable future

1. Introduction

The overuse of fossil fuels in recent decades has resulted in severe increase of CO_2 concentration in atmosphere, leading to global warming and climate change [1-5]. Environmental issues have drawn more and more attention and become one of the most urgent concerns for the public. With the goal for carbon neutrality, researchers all over the world have paid many efforts on CO_2 fixation and conversion to reduce CO_2 concentration in atmosphere [6-11]. Various materials and techniques were applied in CO_2 capture, and great progress has been achieved [12-18]. The utilization of captured CO_2 was more appealing, since CO_2 is not only the major greenhouse gas but also a critical feedstock in chemical industry [19-23]. Therefore, the development of novel catalysts for converting CO_2 into fuels or value-added chemicals is an important research topic nowadays [24-29].

The attempts on CO_2 conversion can be traced back to 1972 when Honda and Fujisima reported TiO_2 for photocatalysis [30]. After the development for several decades, CO_2 conversion has become a prosperous field. Numerous studies of CO_2 conversion by electrocatalysis [31-36], photocatalysis [37-43], photoelectrocatalysis [44-46], thermocatalysis [47-51] and biocatalysis [52,53] have been reported. Diverse nanomaterials

with unique structures were utilized as catalysts. While molecular catalysts are good candidates for CO_2 conversion because of their full contact with CO_2 [54-58], they are often difficult for recycling. In comparison, porous heterogeneous catalysts are of ease to be reutilized [59]. There are several advantages of porous structures for catalytic applications. Firstly, porous structures often possess high specific surface areas, which mean that a high quantity of catalytic sites would be exposed directly to substrates. Secondly, there are abundant channels in the porous structures, which allow for rapid transfer of reactants and products. These advantages are favorable for CO_2 conversion reaction toward the product formation. However, they are mainly in the powder state, meaning that additional procedures such as electrode preparation are required for practical applications of these catalysts [60-66]. Therefore, researchers intended to fabricate porous catalytic membranes that can be utilized directly as electrodes for electrocatalysis and photoelectrocatalysis of CO_2. Apart from the convenience for applications, the binder is not required during the usage of membrane-based catalysts. This should be beneficial to the catalytic performance, since binders generally inhibit the reactivity of catalysts to a certain extent. In addition, reactants can diffuse freely to the surface and inner space of the membranes through abundant channels. Thus, thin porous catalytic membranes often demonstrate higher catalytic site utilization than powder ones. Porous catalytic membranes are a step forward to the device fabrication, providing lots of possibilities on the construction of novel devices for CO_2 conversion (Figure 1).

Here in this review, we summarize recent research progress on the development of porous catalytic membranes for CO_2 conversion. Although tremendous results have been achieved on powder catalysts [67-71], they are excluded from this review because the scope of the review

lies in porous catalytic membranes for CO_2 conversion. In the present review, we discuss the research motivation of catalytic membranes for converting CO_2. Subsequently, we review the widely used methods for preparing catalytic membranes, and describe how these methods be applied to fabricate porous membranes. Then, we highlight the usage of catalytic membranes on several CO_2 conversion techniques, such as electrocatalysis, photocatalysis, photoelectrocatalysis, thermocatalysis, and biocatalysis. We briefly reveal basic rules for every technique used, and summarize the research achievements and current issues. Finally, based on the achieved progress, we provide the outlook and perspective on porous catalysis membranes for CO_2 conversion.

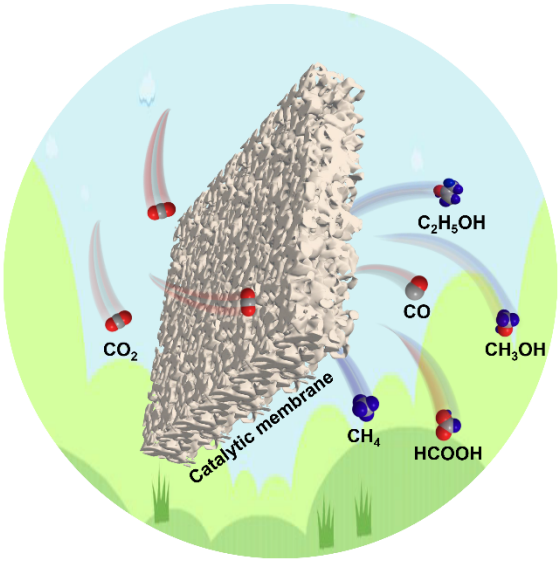

Figure 1. The porous catalytic membranes for CO_2 conversion.

2. Membrane preparation

Porous membranes have been utilized in various fields. While there are a plenty of membrane preparation methods, only a small portion of them can be applied for CO_2 conversion. In this section, we discuss the commonly used preparation methods for the

fabrication of catalytic membranes toward CO_2 conversion.

2.1 Electrochemical method

Up to now, majority of catalytic membranes has been employed as electrodes for electrochemical CO_2 conversion. Therefore, the conductivity of membranes is considered top priority for catalysis performance. Researchers, thus, have paid efforts on fabricating catalytic membranes on metal surface to guarantee high conductivity. Electrochemical method has been widely used in fabricating membrane electrodes. Generally, it consists of electrochemical deposition and anodic etching. For electrochemical deposition, the target matter is deposited onto a substrate driven by applied voltage through redox reaction to obtain a porous film on the substrate surface. While for anodic-etching, metal foils are usually utilized as the anode in an electrochemical cell and etched via electrochemical redox reaction on the anode surface to achieve the porous structure.

Electrodeposition is a common method to prepare porous membranes on metal substrates. Guay et al. reported a porous Bi film electrode through electrodeposition [72]. Firstly, Bi film was potentiostatically deposited on a Ti plate that is unactive during the CO_2 conversion. Then, the as-deposited Bi film was electrochemically oxidized in CO_2-staturated $KHCO_3$ solution, followed by electrochemical reduction in the same electrolyte to obtain electrochemically oxide-derived (EOD) Bi film. Through electrochemical oxidation-reduction, EOD-Bi presented a rough surface and a dramatic increase in electrochemically active surface area. Moreover, porous metal dendrite membranes can be also obtained by the electrodeposition. As reported by Jiao et al, ZnO powder was dissolved in dense KOH solution to prepare the

electrolyte for deposition [73]. Polished Zn foil was employed as the electrode in electrolyte under chronopotentiometry experiment. Under the drive of voltage, Zn precursor in electrolyte was reduced to metallic Zn on foil, affording a porous dendrite Zn film.

In addition to the element metal films, electrodeposition was also applied to fabricate metal alloy membranes, since the synergy between each component contributes to the catalysis performance. Ahn el al. reported a CuAgHg multimetallic thin film for CO_2 conversion [74]. The electrodeposition was represented in Figure 2, where a sulfuric acid solution containing Cu^{2+}, Ag^{+} and Hg^{2+} was employed as the electrolyte. All the metal ions in electrolyte were electrodeposited onto a polished glassy carbon plate under a constant potential. The addition of Hg ion in alloy membrane showed advantage on minimizing hydrogen evolution reaction (HER) and increasing CO_2 conversion selectivity.

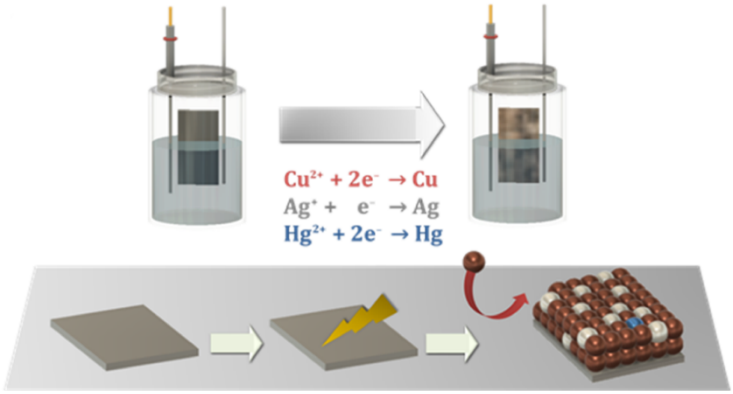

Figure 2. Schematic representation for electrodeposition to form CuAgHg multimetallic film. Reproduced with permission from Ref. [74]. Copyright 2020, American Chemical Society.

Anodic etching is another common method to fabricate porous electrodes. A porous Ag membrane catalyst was reported recently for CO_2 conversion through anodic-etching-reduction method [75]. A polycrystalline Ag foil was firstly applied as the

anode in a two-electrode system with CO_2-saturated $KHCO_3$ electrolyte. An anodic potential was applied on Ag foil to form $AgCO_3$ layer on the surface. The $AgCO_3$ electrode was used directly for CO_2 electrochemical reduction. In the initial stage, $AgCO_3$ would be reduced to porous metallic Ag film, which acts as the catalyst for CO_2 reduction in the following stage.

2.2 Surface coating method

Surface coating is a membrane fabricating method where a precursor solution/colloid is evenly coated on the substrate followed by post-treatment to synthesize the target membrane. According to the precursor coating method, surface coating can be categorized into dip-coating, drop-coating, blade-coating, sol-gel coating, etc. Through surface coating, high-quality target membranes can be achieved on the surface of substrates. In the past decade, there were some reports on preparing catalytic membranes coated on the surface of substrates. In general, a continuous and uniform thin membrane can be obtained on the substrate surface.

Kubiak et al. employed an iron porphyrin covalent organic framework (COF) to construct catalytic membranes through dip-coating [76]. Carbon cloth was used as the substrate, which was initially dipped into 5,10,15,20-tetra-(4-aminophenyl)-porphyrin Fe(III) chloride (FeTAPPCl) solution. After drying the carbon cloth in the air, 2,5-dihydroxyterephthalaldehyde (Dha) solution was added to its surface. Then, the system was placed under 140 ℃ for FeTAPPCl reacting with Dha to form the COF thin film on carbon cloth. The as-prepared COF film can be directly employed for electrochemical CO conversion.

Hot-drop coating is similar to dip-coating. The difference lays in that each component is

dropped alternatively in dip-coating method, while all the components are dropped once onto the substrate surface in hot-drop coating. Hot-drop coating was applied by Bocarsly et al. to prepare Cr-Ga thin film [77]. Glassy carbon was used as the substrate and heated to 120 ℃ initially. Then, $Cr(NO_3)_3$ and $Ga(NO_3)_3$ mixed solution was drop-casted onto the surface. After drying, the glassy carbon plate was sintered in Ar/H_2 atmosphere to get Cr-Ga thin film ready for CO_2 electrolysis.

Different from dip-coating and hot-drop coating approaches, a doctor blade was used to obtain a smooth film after dropping precursor solution onto the substrate surface in blade-coating method. As reported by Kamat and coauthors, TiO_2 paste was dropped onto fluorine doped tin oxide (FTO) plate surface, and a doctor blade was employed to obtain a flat film surface [78]. The TiO_2 coated FTO plate was obtained after drying in low temperature and annealing at high temperature in sequence.

Sol-gel coating is another typical surface coating method employed to fabricate catalytic membranes. Maroto-Valer et al. reported a TiO_2 coated glass strip for CO_2 conversion by this method [79]. Titanium (IV) n-butoxide and glacial acetic acid were mixed together, and deionized water was added into the mixture in a single step. After aging overnight, polypropylene glycol was dropped into the mixture to gain TiO_2 sol-gel. Glass strip was soaked in TiO_2 sol-gel for a period of time and then withdrawn out. After calcination, the TiO_2 coated glass was finally obtained.

2.3 Filtration assembly method

Filtration has been evolved as a new method to fabricate catalytic membranes. Typically,

some nanomaterials, especially for nanowires, can be filtered onto porous membranes to assemble nonwoven films. The filtered films can either be employed as catalytic membranes directly for CO_2 conversion or be utilized as the precursor to fabricate catalytic membranes.

In a work reported by Broekmann et al., Cu nanowires (Cu-NWs) were synthesized without using surfactants [80]. Cu-NWs were subsequently vacuum-filtered onto Nylon cloth, forming Cu-NWs assembly (Figure 3). When the Cu-NWs/Nylon was soaked in water, light Cu-NWs assembly floated on the water surface, while Nylon fell down to bottom. Finally, a supporting substrate was used to pick up floating Cu-NWs assembly. After photonic curing process, the as-prepared Cu-NWs were firmly attached onto the substrate and ready for catalytic uses. In addition, there is another report on preparing enzyme decorated porous membranes by filtration for CO_2 conversion [52]. In this work, three enzymes (i.e., formate dehydrogenase (FDH), formaldehyde dehydrogenase (FaldDH) and alcohol dehydrogenase (ADH)) were filtered onto ultrafiltration membranes. These enzymes were firmly immobilized onto the substrate surface and would not dissolve again. The obtained system presented nice catalysis performance on CO_2 conversion to methanol.

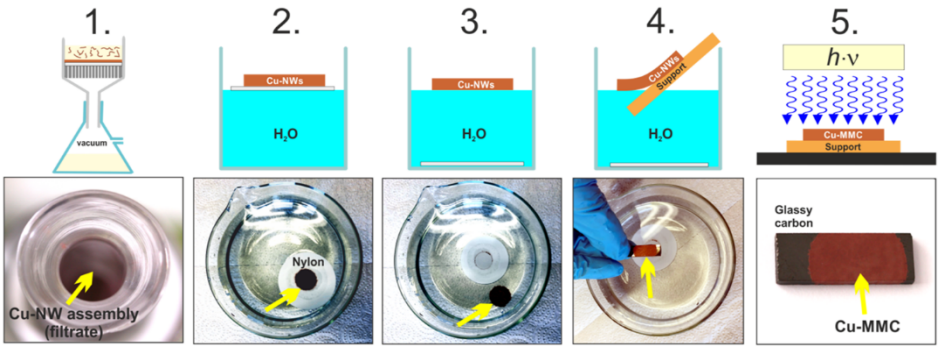

Figure 3. Schematic representation for preparing Cu-NWs assembly through vacuum filtration. Reproduced with permission from Ref. [80]. Copyright 2019, American Chemical Society.

We employed filtration method to prepare a hybrid metal-organic framework (MOF) film for CO_2 conversion (Figure 4) [81]. Firstly, copper hydroxide nanostrands (CHN) were prepared as the MOF precursor. A fullerene derivative ($PC_{61}BM$) self-assembled onto CHN driven by electrostatic attraction. Then, vacuum filtration was applied to obtain hybrid CHN film on porous membrane. Subsequently, hybrid CHN film was soaked in meso-tetra(4-carboxyphenyl)porphine (TCPP) solution, and CHN would react with TCPP to form the MOF film where $PC_{61}BM$ was embedded in the MOF film in situ. This method presents the generality for various MOF film preparations and shows advantage on encapsulating functional components inside the MOF film.

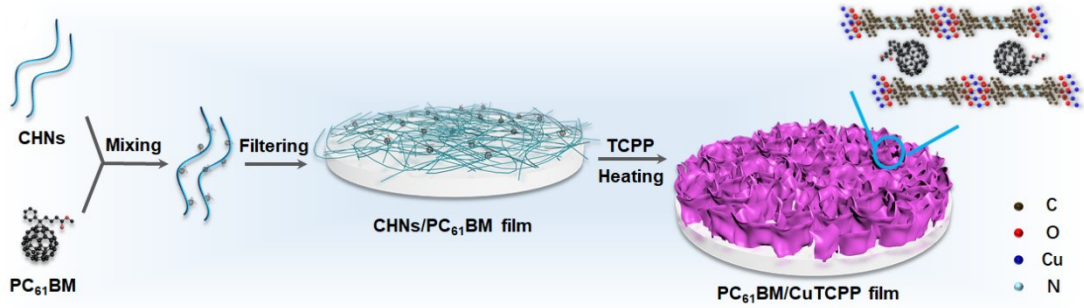

Figure 4. Illustration for the fabrication of $PC_{61}BM$/CuTCPP film by filtration. Reproduced with permission from Ref. [81]. Copyright 2021, Royal Society of Chemistry.

2.4 Others

Apart from the aforementioned methods, some novel protocols emerge for catalytic membrane preparation. Sintered metal method was employed in the fabrication of porous catalytic Ni membrane, reported by Kim and coworkers [82]. Alumina-modified nickel powders with particle size about 3 μm were pressed into a pellet without any binder under

high pressure of 70 MP. Afterwards, the pellet sample was sintered at high temperature of 900 ℃ in reductive atmosphere. The as-prepared Ni membrane presented a porous morphology and could be used as a catalytic membrane reactor for CO_2 conversion with H_2O to CH_4.

Buonsanti et al. reported a method to construct MOF-based hybrid film named as Ag@Al-PMOF [83]. Ag nanocrystals (Ag NCs) were drop-casted onto the substrate surface in the first step. Atomic layer deposition (ALD) was applied to deposit Al_2O_3 shell onto Ag NCs. The Al_2O_3 shell would react with TCPP ligand to form Al-PMOF film, while Ag NCs were completely embedded in the MOF film (Figure 5). The hybrid Ag@Al-PMOF film demonstrated a good property on the suppression of hydrogen evolution reaction.

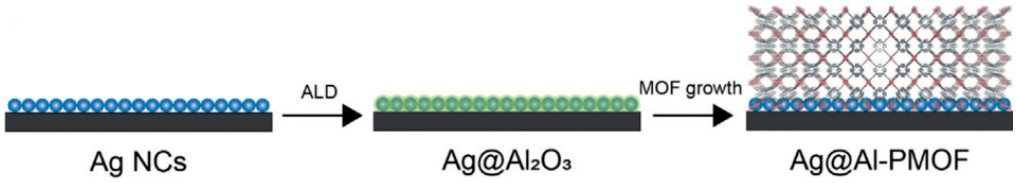

Figure 5. Illustration for the fabrication of Ag@Al-PMOF film. Reproduced with permission from Ref. [83]. Copyright 2019, Wiley-VCH.

An electrospinning-carbonation method was employed by He et al. to synthesize porous carbon membranes [84]. The procedure was illustrated in Figure 6. They used ZIF-8 as a carrier to convey Cu atom. $Cu(NO_3)_2$ was injected into ZIF-8 solution. After ultrasonication and stirring, the obtained Cu/ZIF-8 particles were separated by centrifugation and dried overnight. Cu/ZIF-8 solution was electrospun onto a polymer fiber membrane, followed by carbonization to form porous carbon fiber-based membrane under Ar atmosphere. After cooling, H_2SO_4 solution was used to wash out Cu nanoparticles and residual Zn in the

as-prepared membrane to obtain Cu single atom decorated through-hole carbon nanofiber membranes (CuSAs/TCNFs).

Figure 6. (a) Schematic representation for the synthesis of CuSAs/TCNFs membranes. (b) Photos of CuSAs/TCNFs membranes. Reproduced with permission from Ref. [84]. Copyright 2019, American Chemical Society.

Table 1. Summary of catalytic membranes and their catalysis performance. j: geometric current density, FE: Faradaic efficiency. TOF: turnover frequency.

Catalytic membrane	Preparation	Reactant	Main product	Catalysis method	Performance	Ref.
UiO-66 film/Ag flat	Drop-casting	CO_2	CO	Electroreduction	$j_{CO} \approx$ -1.5 mA cm^{-2} at -1.0 V vs. RHE	23
Bi_2O_3 film	Electrodeposition	CO_2	HCOOH	Electroreduction	j_{HCOOH} = -8.3 mA cm^{-2}, 0.9 V overpotential	72
Zn film	Electrodeposition	CO_2	CO	Electroreduction	-0.7 V overpotential	73
CuAgHg film	Electrodeposition	CO_2	C_2 species	Electroreduction	32% ethanol, 41% C_2 (ethanol + ethylene)	74
Ag film	Anodic etching	CO_2	CO	Electroreduction	FE_{CO} = 90% at overpotential 0.29 V	75
COF/carbon cloth	Dip-coating	CO_2	CO	Electroreduction	FE_{CO} = 80%, TOF > 600 h^{-1} mol^{-1}	76
Cr-Ga film	Drop-coating	CO_2	Oxalate	Electroreduction	$FE_{oxalate}$ = 59 ± 3%, 0.69 V overpotential	77
TiO_2/FTO film	Blade-coating	CO_2	Methanol	Electroreduction	$FE_{methanol} \approx$ 90% at -2.0 V	78

Cu nanowire film	Filtration	CO_2	C_2H_4	Electroreduction	$FE_{ethylene}$ = 42.4% at -1.1 V	80
Ag@Al-PMOF film	ALD-solvothermal method	CO_2	CO	Electroreduction	55.8% selectivity CO at -1.1 V	83
Cu/carbon fiber film	Eletrospin-carbonization	CO_2	Methanol	Electroreduction	$FE_{methanol}$ = 44%, -93 mA cm^{-2}	84
Porous Cu-DAT film	Electrodeposition	CO_2	C_2H_4/C_2H_5OH	Electroreduction	$FE_{ethylene}$ = 40%, $FE_{ethanol}$ = 20% at -0.5V	85
Cu/Nu-1000 film	Solvothermal deposition	CO_2	HCOOH	Electroreduction	FE_{HCOOH} = 31% at -0.82 V	86
Porous Pt film	Dual-templating approach	CO_2	Alcohol	Electroreduction	$FE_{alcohol}$ = 23.9%, yield 2.1×10^{-8} mol s^{-1} cm^{-2} at 51 mA/cm^{-2}	87
Cu nanowire film	Annealing-electorreduction	CO_2	C_2H_5OH, CO, C_2H_4, n-Propanol	Electroreduction	$FE_{ethylene}$ = 20.3%	88
PDA film	oCVD	CO_2	HCOOH, CO	Electroreduction	j_{geo} = 18 mA cm^{-2} at 0.21 overpotential	89
Au/nanoPE membrane	Deposition	CO_2	CO	Electroreduction	$FE_{CO} \approx 92\%$, $j_{geo} \approx 25.5$ mA cm^{-2} at -0.6 V	90

Porous carbon film	MOF-carbonization	CO_2	Methanol, CO	Electroreduction	Yield = 90.17 μmol g^{-1} h^{-1}	91
TiO_2 film	Sol-gel	CO_2	CO, CH_4	Photoreduction	$Yield_{CO}$ ≈ 1.3 μmol g^{-1} h^{-1}, $Yield_{methane}$ ≈ 1.3 μmol g^{-1} h^{-1}	79
C_3N_4-TiO_2/Nafion film	Solvent evaporation	H_2O/CO_2	Methanol	Photoreduction	Yield = 61 μmol g_{cat}^{-1} h^{-1}	92
Cu-TiO2/ZIF-8 film	Surface doping	CO_2	Methanol, CO	Photoreduction	$Yield_{methanol}$ = 28.8 ± 2.6 ppm, $Yield_{CO}$ = 16.3 ± 0.7 ppm	93
ZnSi/SiO_2 film	Liquid-phase epitaxial growth	CO_2	CO	Photoreduction	Yield = 126.7 μmol g_{cat}^{-1} h^{-1}	94
$PC_{61}BM$/CuTCPP	Filtration	CO_2/epoxide	Carbonate	Photocatalysis	Conversion = 92.4%, TOF = 36.0 h^{-1}	81
Nanoporous Au mesh	Electrochemical oxidation and reduction	CO_2	CO	Photoelectroreduction	FE_{CO} = 90%, -2.94 mA cm^{-2} at -0.11 V	44
TiO_2/Ag/n-GaN	E-beam evaporator	CO_2	HCOOH	Photoelectroreduction	$Yield_{HCOOH}$ = 62 μmol cm^{-2} h^{-1}	45

PSS:PEDOT/Cu_2O/FTO film	Electrodeposition	CO_2	Methanol	Photoelectroreduction	0.495 μmol L^{-1} of methanol formation	46
Pb/CuO/Cu_2O film	Photo-assisted electrodeposition	CO_2	Methanol, HCOOH, CO	Photoelectroreduction	FE = 40.45%	95
Cu/Zn alloy film	Electrodeposition	CO_2	Methanol	Photoelectroreduction	FE = 60%	96
MOF film/aerogel	Secondary growth	CO_2/epoxide	phenyl cyclic carbonate	Thermochemical	Conversion = 91.5%	36
Porous Ni membrane	Sintered metal method	$(H_2O/CO_2)/CH_4$	Syngas	Thermochemical	Syngas production rate of 5.68×10^{-2} N m^3 h^{-1}	82
Enzymes/porous membrane	Filtration	CO_2	Methanol	Biocatalysis	Yield = 0.074 μmol cm^{-2}	52
CA/TiO_2/PVDF film	Sol-gel method	CO_2	$CaCO_3$	Biocatalysis	110 mg $CaCO_3$ / mg enzyme	53

3. Catalysis for CO_2 conversion

In this section, we discuss the applications of porous catalytic membranes for CO_2 conversion. Compared to powder-state catalysts, catalytic membranes present advantage on the recyclability and suitability of device fabrication. We summarize recent studies on catalytic membranes in Table 1 [23,36,44-46,52,53,72-96].

3.1 Electrochemical catalysis for CO_2 conversion

Electroreduction of CO_2 has become one of the hottest topics for converting CO_2 to value-added fuels and chemicals. Electrocatalysis for CO_2 reduction presents a series of advantages. It is able to restore intermittent electricity into chemical energy [97-99], without requirements for H_2 feedstock. In addition, the CO_2 electroreduction can procced in a large temperature range from room temperature to several hundred degrees centigrade. Meanwhile, reduction products can be tuned by adjusting electrocatalysts, electrolytes, applied voltage, etc. Nevertheless, the electroreduction for CO_2 conversion is a complex process. The diversity of reduction pathways leads to various products, such as CO, HCOOH, methanol, ethanol, CH_4, and C_2H_4. Reduction processes of corresponding products were summarized in Table 2. However, there are still some challenges in the CO_2 electroreduction. The competitive reactions such as HER are still evitable, which result in low Faradaic efficiency. The product selectivity also needs further improvements.

Table 2. CO_2 reduction processes with corresponding products and potentials.

Reactions	Potential (V vs RHE)
CO_2 (g) + $2H^+$ + $2e^-$ → HCOOH (l)	-0.250
CO_2 (g) + $2H^+$ + $2e^-$ → CO (g) + H_2O (l)	-0.106
CO_2 (g) + $4H^+$ + $4e^-$ → HCHO (l) + H_2O (l)	-0.070
CO_2 (g) + $6H^+$ + $6e^-$ → CH_3OH (l) + H_2O (l)	0.016
CO_2 (g) + $8H^+$ + $8e^-$ → CH_4 (g) + $2H_2O$ (l)	0.169
CO_2 (g) + $12H^+$ + $12e^-$ → C_2H_4 (l) + $4H_2O$ (l)	0.064
CO_2 (g) + $12H^+$ + $12e^-$ → C_2H_5OH (l) + $3H_2O$ (l)	0.084
CO_2 (g) + $18H^+$ + $18e^-$ → $CH_3CH_2CH_2OH$ (l) + $5H_2O$ (l)	0.210

Metallic oxides are common materials for electroreduction of CO_2. Kamat et al. prepared a nanostructured TiO_2 film via blade coating method [78]. The as-prepared TiO_2 film was applied as a working electrode in a two-component electrochemical cell with Pt as the counter electrode, Ag/Ag^+ (0.55V vs NHE), and tetraethylammonium perchlorate/acetonitrile as the electrolyte. CO_2 was purged into cathodic component for 30 min before the test. They proved that the conversion from Ti^{4+} to Ti^{3+} at a potential more negative than -0.95 V (vs NHE) contributed to the electroreduction of CO_2 (Figure 7).

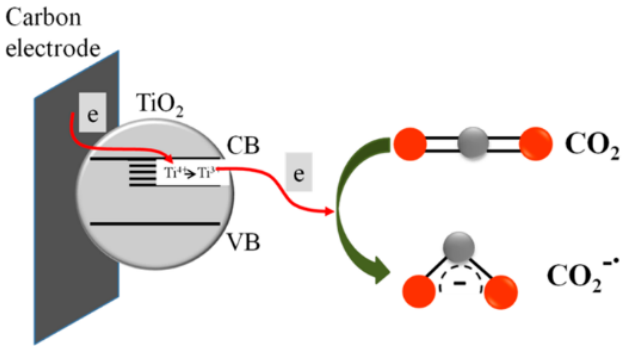

Figure 7. Electrochemical conversion of Ti^{4+} to Ti^{3+} and electron transfer from Ti^{3+} to CO_2 resulting in $CO_2^{-\bullet}$. Reproduced with permission from Ref. [78]. Copyright 2014, American

Chemical Society.

As discussed above, an Ag@Al-PMOF hybrid film was synthesized by Buonsanti and coworkers [83], where Ag NCs were embedded inside the MOF film. The authors measured its CO_2 electroreduction performance in a CO_2-saturated $KHCO_3$ solution. They found that the film can dramatically increase the selectivity of Ag NCs on CO_2 conversion toward CO as compared to bare Ag NCs (Figure 8). The film can protect Ag NCs during CO_2RR and improve the morphology stability. In addition, the synergistic effect of minor mass transfer by porous MOF layer and electron transfer in Ag@Al-PMOF interfaces enhanced the electrocatalysis performance of the hybrid film.

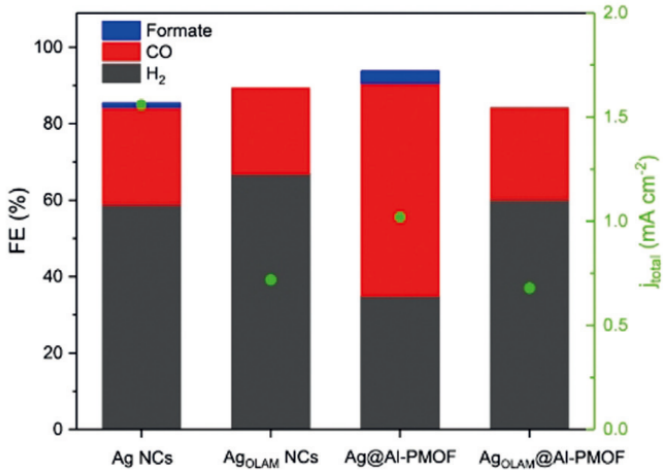

Figure 8. Faradaic efficiency and total current density for Ag NCs and Ag@Al-PMOF catalysts, with and without oleylamine (OLAM) ligand, measured at 1.1 V vs RHE. Reproduced with permission from Ref. [83]. Copyright 2019, American Chemical Society.

He et al. prepared a catalytic single atom decorated porous carbon fiber membrane, namely CuSAs/TCNFs [84]. The electrochemical catalysis performance was tested in

CO_2-saturated $KHCO_3$ solution in an undivided cell. Methanol was detected as the CO_2 reduction product by CuSAs/TCNFs, while CO or HCOOH was produced by other single-atom metal catalysts in aqueous solution. The as-prepared porous carbon fiber provided abundant single Cu atom catalysis sites and mass transfer channels. The synergy of through-hole carbon fiber structure and distributed single Cu sites endowed CuSAs/TCNFs with the Faradaic efficiency of 44 % for CO_2 conversion to methanol (Figure 9).

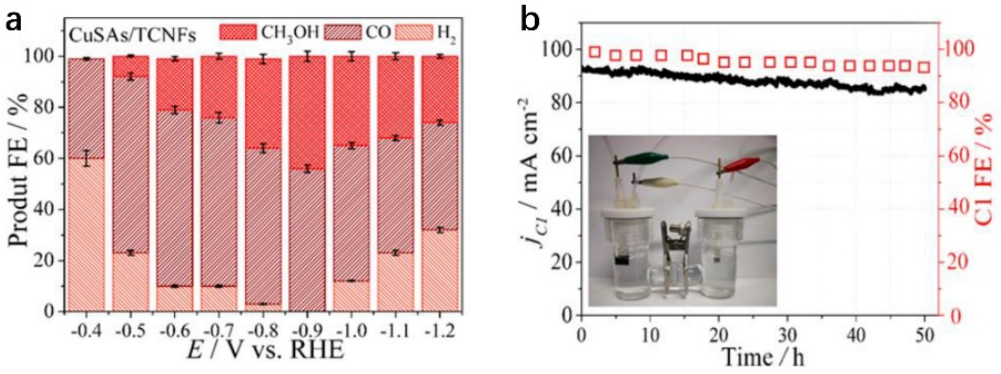

Figure 9. (a) Faradaic efficiency of the products by CuSAs/CNFs. (b) Long-term tests of CuSAs/TCNFs performed at -0.9 vs RHE. Reproduced with permission from Ref. [84]. Copyright 2019, American Chemical Society.

Transition metals have long been used as electrocatalysts for CO_2 reduction. Macfarlane et al. fabricated hierarchically ordered Pt nanochannel array (HPNA) membrane with porosity and pore size of 32.5% and 2.5 nm, respectively, by template approach [87]. CO_2 conversion was conducted in a two-chamber cell with the electrolyte of 1 M Na_2CO_3 solution, where CO_2 was bubbled into the cell through HPNA (Figure 10a). Methanol was first observed at -0.63 V (vs RHE), and the Faradaic efficiency and alcohol production yield were up to 23.9% and 2.1×10^{-8} mol s^{-1} cm^{-2} at -2.05 V (vs RHE), respectively (Figure 10b-d). The good performance

was contributed to three-dimensional microchannel interfaces and highly mesoporous active surface area of HPNA. However, there was HER along with CO_2 reduction reaction (CO_2RR), resulting in low Faradaic efficiency for CO_2 conversion. Nowadays, some catalysts were fabricated into membranes or films to serve as binder-free and less resistive electrodes directly.

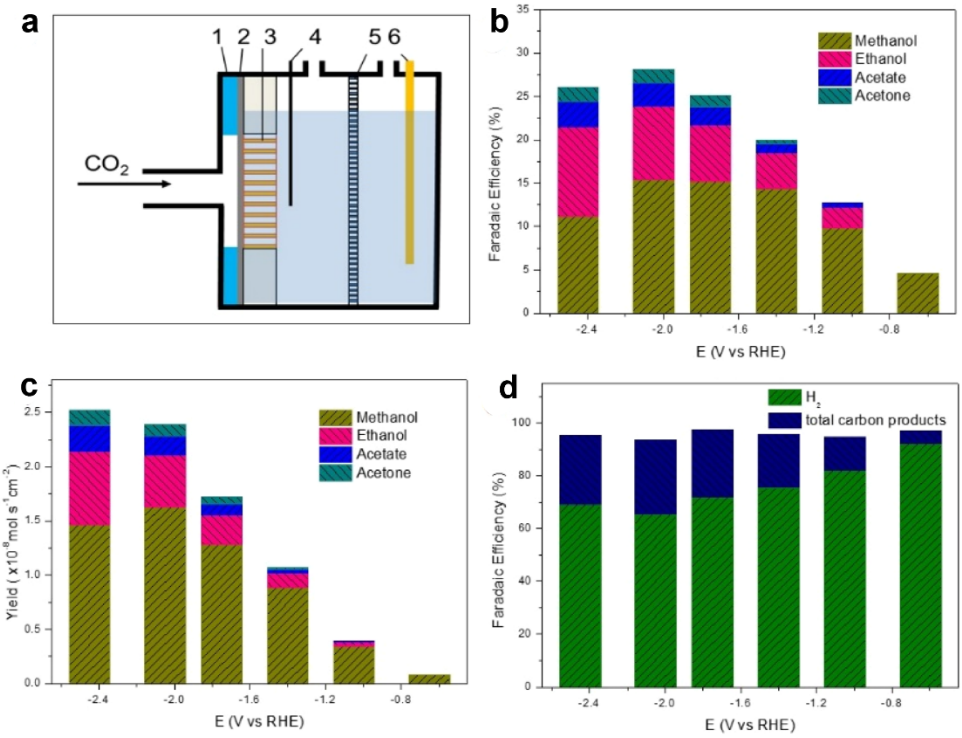

Figure 10. Electrochemical conversion of CO_2 using HPNA as a flow-through membrane reactor. (a) Schematic diagram of the cell: (1) spacer, (2) stainless steel mesh support, (3) HPNA reactor, (4) reference electrode, (5) Nafion membrane, and (6) counter electrode. Reduction potential-dependent Faradaic efficiency (b) and yield (c) for CO_2 reduction. (d) Total carbon products and hydrogen yield as a function of potential. Reproduced with permission from Ref. [87]. Copyright 2018, American Chemical Society.

In a recent study, Smith et al. prepared Cu nanowire arrays on Cu foil substrate [88].

They studied the influence of Cu nanowire morphology on electrochemical reduction of CO_2, showing that the selectivity from the electrochemical reduction of CO_2 can be tuned by adjusting Cu nanowire length. As presented in Figure 11, n-propanol was detected alone with CO, HCOOH and C_2H_4 when the Cu nanowire length was higher than 2.4 ± 0.6 μm. When Cu nanowires were longer than 7.3 ± 1.3 μm, C_2H_6 was among the products. They also noted that the increase on the length and density of Cu nanowires could result in the rise of selectivity for C_2H_4 due to the formation of C_2H_4 through a CO coupling mechanism. The as-prepared Cu nanowire film achieved the Faradaic efficiency up to 20.3% for C_2H_4, which was about half of the value for the Cu nanowire film prepared by the filtration [80], indicating that the preparation process can influence the performance of catalytic membranes.

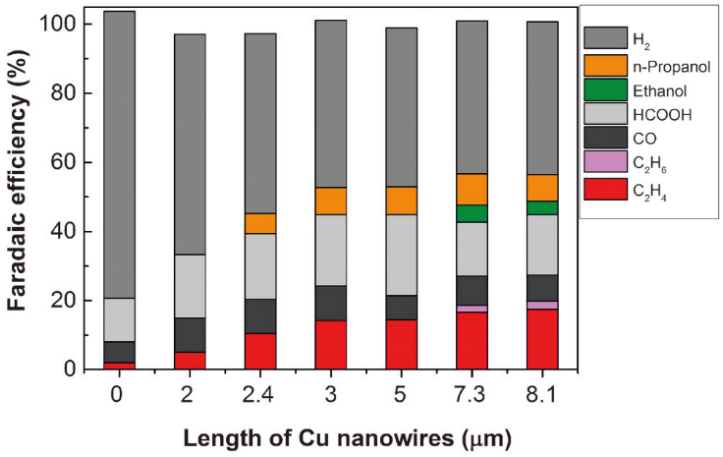

Figure 11. Faradaic efficiency for C_2H_4, C_2H_6, CO, HCOOH, ethanol, n-propanol, and H_2 on Cu nanowire arrays with different lengths at -1.1 V vs RHE in CO_2-saturated 0.1 m $KHCO_3$ electrolyte (0 mm nanowire represents Cu foil). Reproduced with permission from Ref. [88]. Copyright 2016, Wiley-VCH.

Recently, a metal-free organic electrocatalyst, i.e., polydopamine (PDA), was reported by Stadler and coworkers [89]. Oxidative chemical vapor deposition (oCVD) was employed to

create conductive conjugated PDA on carbon felt or FTO glass. Electroreduction of CO_2 was conducted in a three-electrode system in a H-cell configuration with 0.1 M tetrabutylammonium hexafluorophosphate in acetonitrile-water as the electrolyte. PDA coated FTO or carbon felt demonstrated good catalytic performance with geometric current density of 18 mA cm^{-2} at -0.86 V (vs NHE), which is lower than state-of-the-art metal electrocatalysts (e.g., Ag catalyst). The Faradaic efficiency for the electrosynthesis of C_1 species (such as HCOOH and CO) was higher than 80% (Figure 12). They proved that the CO_2 electroreduction performance was contributed by interactions between CO_2 and nucleophilic hydrogen-bonded active sites of PDA.

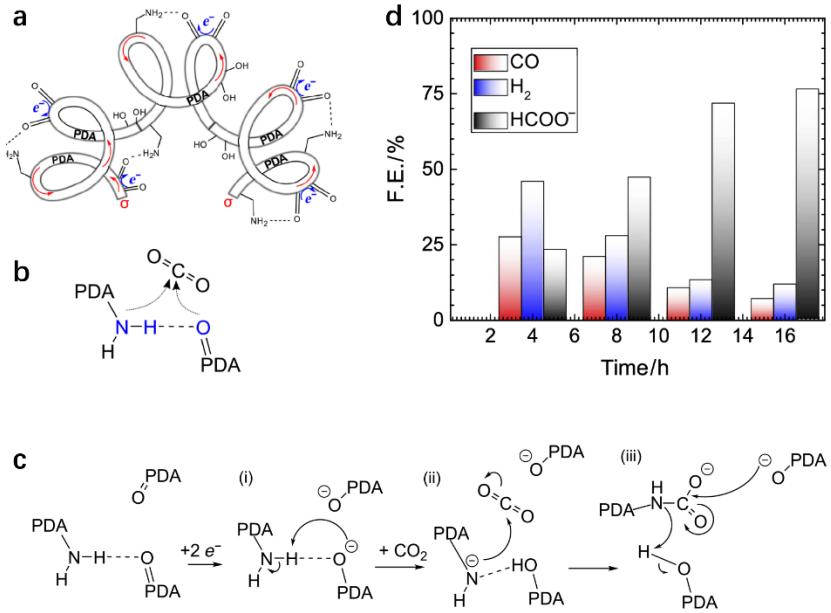

Figure 12. (a) Electrocatalytic PDA wires consisting of a conductive conjugation body with functional groups on a carbon-based carrier electrode. (b) Two-spot delocalized amine-carbonyl hydrogen-bonded catalytic center on PDA. (c) Initial steps driving CO_2RR in conductive PDA: (i) electrochemical activation of the hydrogen-stabilized carbonyl group, (ii) subsequent formation of a nucleophilic center via the adjacent amine, and (iii) attachment to

CO_2 creating an amide. (d) Faradaic efficiencies of CO, H_2, and formate as a function of time. Reproduced with permission from Ref. [89]. Copyright 2017, American Association for the Advancement of Science.

In another case, Dumée et al. reported a carbon-based membrane as an electrochemical reactor derived from a MOF [91]. MOF-derived carbon membrane can maintain its microporous structure and easily introduce metal atoms into the membrane. 1-Butyl-3-methylimidazolium hexafluorophosphate ionic liquid in dimethylacetamide was employed as the electrolyte to study the CO_2 conversion. The authors proved that the selectivity and yield of products can be tuned by switching the dopped metal ions. The carbonized product at 700 °C (i.e., C-ZnZIF700) exhibited high methanol yield of 90 μmol g^{-1} h^{-1} (Figure 13). When Cu was introduced to the catalyst, the resulted C-CuZnZIF700 showed relatively lower methanol production of 67 ± 17 μmol g^{-1} h^{-1} with an additional CO yield of 0.11 μmol g^{-1} h^{-1}. Moreover, methanol would be the only product when adding Ni to C-ZnZIF700 (i.e., C-NiZnZIF700), but the yield was down to 22 ± 8 μmol g^{-1} h^{-1}.

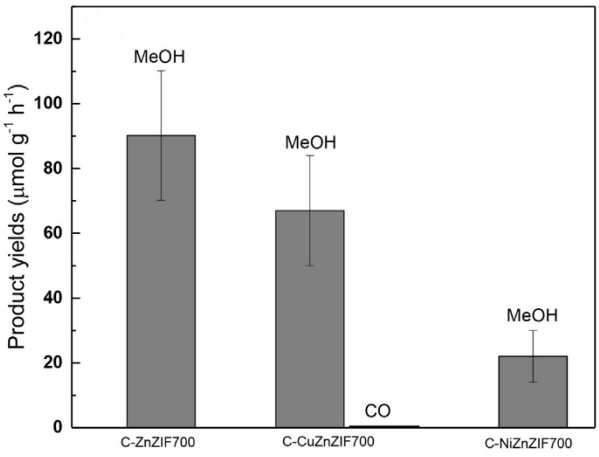

Figure 13. Impact of metal ion composition on the electrocatalytic conversion yields. Reproduced with permission from Ref. [91]. Copyright 2019, Elsevier.

3.2 Photochemical catalysis for CO_2 conversion

Photocatalysis of CO_2 conversion is regarded as an appealing path on account of the clean and inexhaustible solar energy used [100-104]. It generally involves with three procedures: 1) CO_2 adsorption to photocatalysts, 2) photogenerated electron-hole (e-h) separation, and 3) surface CO_2 conversion. The products such as CO, HCOOH, CH_3OH, and CH_4 vary according to the band structure of photocatalysts [105-109]. In addition, CO_2 can also be incorporated into organic molecules for producing value-added chemicals, like carbonates, carboxylates, and carbamates. However, the low photocatalytic efficiency still hindered the application of this method. Thus, lots of efforts have been paid to the enlargement of light adsorption range and construction of porous catalyst structures to convey more active sites [110,111]. It is also proven that built-in electricity field, defect states and surface polarization favored the e-h separation and enlarged the lifetime of photogenerated carriers, leading to the improvement of photocatalysis efficiency [112-114]. Based on these studies, several photocatalytic membranes have been utilized for CO_2 conversion, which presented not only outstanding performance, but also advantages on recycling and stability.

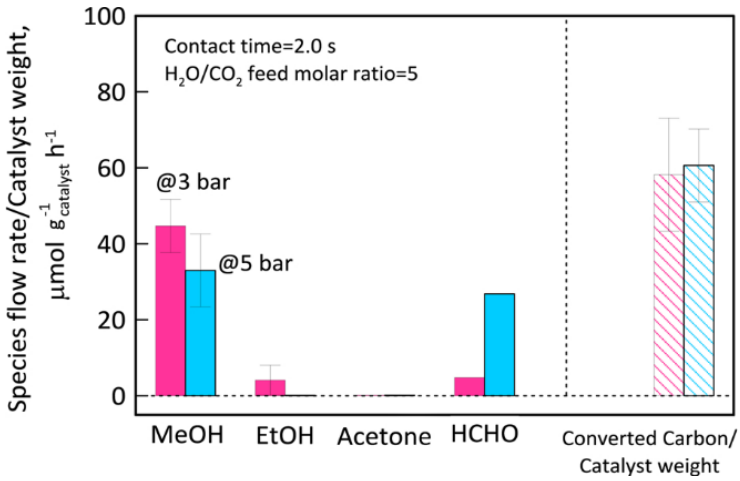

Figure 14. Species flow rate and converted carbon / catalyst weight at 3 and 5 bar. Reproduced with permission from Ref. [92]. Copyright 2019, Elsevier.

TiO_2 is a classic photocatalyst. In a recent work, Barbieri et al. prepared a C_3N_4-TiO_2 embedded Nafion membrane for photoreduction of CO_2 [92]. A continuous reaction facility equipped with the C_3N_4-TiO_2/Nafion membrane was set up under UV irradiation for CO_2 photoreduction. They proved that higher H_2O/CO_2 feed molar radio could lead to increased methanol production with a selectivity higher than 83%. Because of the heterojunction in C_3N_4-TiO_2, the composite membrane showed an enhanced photocatalysis property with total carbon conversion of 61 μmol $g_{catalyst}^{-1}$ h^{-1} (Figure 14).

In a different study, Dumée et al. reported a Cu-TiO_2 nanoparticle-doped ZIF-8 membrane for CO_2 conversion [93]. They evaluated the photocatalysis efficiency of as-prepared hybrid membrane under UV irradiation. Methanol and CO were the only products detected. The highest yields of Cu-TiO_2/ZIF-8 membrane for methanol and CO were 2,238 and 2,170 ppm g_{cat}^{-1} respectively, thanks to the high CO_2 adsorption by MOF and high reactivity of photoexcited electrons generated by Cu-TiO_2 (Figure 15). The authors also highlighted the critical role of solvent in CO_2 reduction. A Lewis acid solvent, dimethylacetamide, was favorable for CO_2 photoconversion, attributed by more intimate interaction with CO_2.

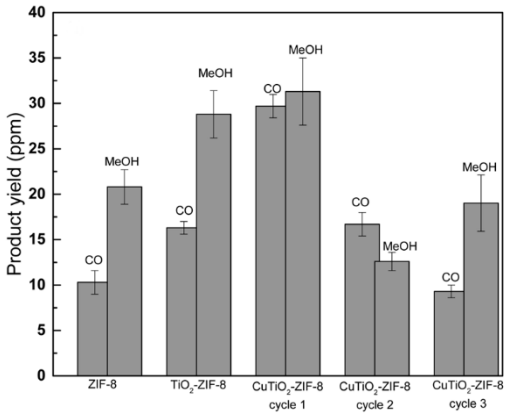

Figure 15. Effect of membrane composition on the product yield. Reproduced with permission from Ref. [93]. Copyright 2017, American Chemical Society.

A clay-like layered zinc silicate (LZS) nanosheet film was synthesized by Wand et al. through liquid-phase epitaxial growth [94]. Photocatalysis performance of LZS was measured in a transparent reactor with CO_2 and H_2O vapor pumped into the system. LZS was placed inside the photoreactor under light beam of Xe lamp. CO was the major product from the CO_2 conversion. The two-dimensional architecture of LZS could afford an engineered surface with a surface area of 185.4 m^2 g^{-1}, leading to high active sites. Through density functional theory (DFT) calculations, they found that free energy of forming adsorbed *COOH over LZS is a key step in CO_2 reduction (Figure 16), which is close to that of other metal-free systems. Therefore, LZS exhibited nice CO_2 photoreduction performance with CO evolution rate of 126.7 μmol g^{-1} h^{-1}.

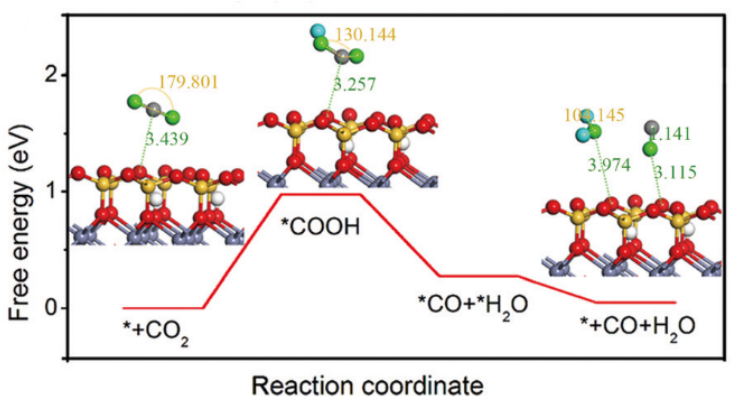

Figure 16. Free energy diagram for the reduction of CO_2 to CO on LZS (001). Reproduced with permission from Ref. [94]. Copyright 2019, Wiley-VCH.

Catalyzing CO_2 cycloaddition with epoxides is of promise for CO_2 fixation. However, the reaction usually proceeds under high temperature and high pressure [115-118]. To conquer this issue, in a recent study, we reported a hybrid MOF film, i.e., $PC_{61}BM$/CuTCPP, for photocatalytic CO_2 cycloaddition to epoxides [81]. The catalytic hybrid film was tested in acetonitrile with tetrabutylammonium bromide as a cocatalyst under simulated sunlight irradiation. We conducted thorough experiments to understand the influence of membrane thickness, substituent groups of epoxides and $PC_{61}BM$ concentration on the photocatalysis performance of $PC_{61}BM$/CuTCPP membrane. The porous structure and photogenerated electron migration between $PC_{61}BM$ and CuTCPP could dramatically improve the catalysis performance of the hybrid membrane (Figure 17). Thus, CO_2 cycloaddition to epoxides was realized under ambient conditions (room temperature and 1 atm pressure) with high epichlorohydrin conversion and TOF of 92.4% and 36.0 h^{-1}, respectively.

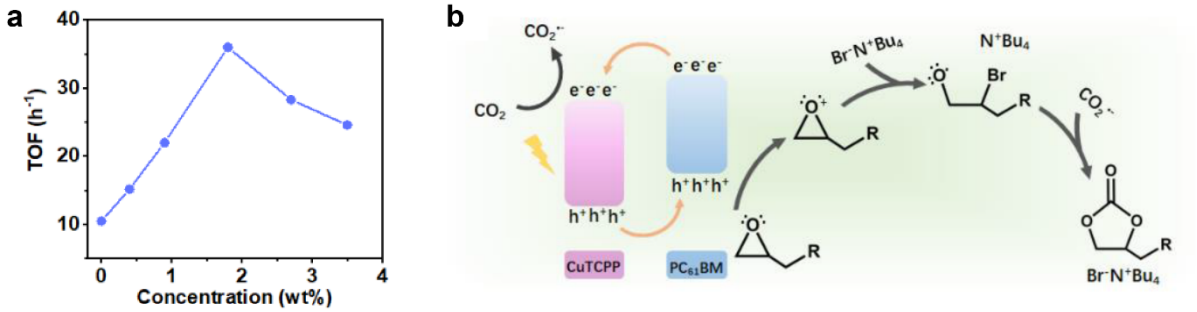

Figure 17. (a) TOF of $PC_{61}BM$/CuTCPP film with various $PC_{61}BM$ concentrations. (b) Proposed reaction mechanism for CO_2 conversion. Reproduced with permission from Ref. [81]. Copyright 2021, Royal Society of Chemistry.

3.3 Photoelectrochemical catalysis for CO_2 conversion

Photoelectroreduction of CO_2 is more attractive since the bias potential on photoelectrocatalysts could facilitate the e-h separation. Semiconductors are usually chosen for being as photoelectrodes. Generally, p-type semiconductors are utilized as photocathodes for CO_2 reduction, while n-type semiconductors as photoanodes for H_2O oxidation [45,119]. Like electrocatalysis and photocatalysis, there is also a wide range of products, such as CO, HCOOH, and methanol, generated from the photoelectrocatalysis of CO_2. The selectivity of reduction products can be tuned by the combination of materials for anodes and cathodes [120]. However, the photoelectrochemical CO_2 conversion is still in its initial stage and the stability of photoelectrodes requires a further improvement because of the photo-corrosion.

Zaboni et al. reported a poly(3,4-ethylenedioxythiophene) polystyrene sulfonate (PEDOT:PSS) coated Cu_2O/FTO photoelectrode for CO_2 reduction [46]. They studied photoelectroreduction of CO_2 in various support electrolytes, such as $NaHCO_3$/Na_2CO_3 buffer, Na_2CO_3, and Na_2SO_4, and the influence of membrane thickness on the performance for CO_2

conversion. According to the mechanism shown in Figure 18, the as-prepared FTO/Cu_2O/PEDOT:PSS exhibited methanol production rate of 460 μmol L^{-1} after 60 min of reaction in $NaHCO_3$/Na_2CO_3 under UV-Vis light and applied potential of 0.0 V vs Ag/AgCl. The photoelectrode also presented an enhanced stability due to the protection by the PEDOT:PSS layer.

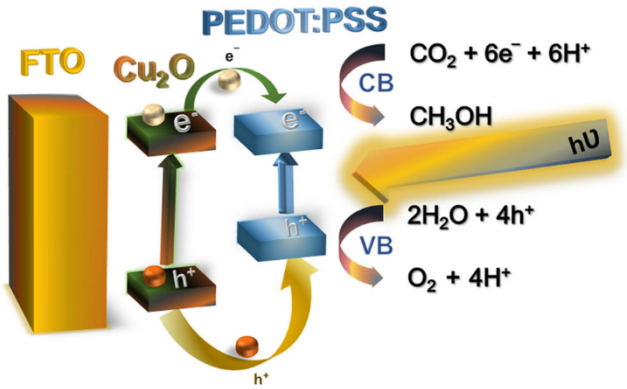

Figure 18. Schematic representation of the CO_2 reduction mechanism by FTO/Cu_2O/PEDOT:PSS. Reproduced with permission from Ref. [46]. Copyright 2021, Springer.

Metallic oxides are another typical type of materials applied for photoelectrochemical catalysis. Metal-decorated CuO/Cu_2O layered thin film was fabricated by Woo et al. for CO_2 photoelectroreduction under visible light [95]. The deposited metal on CuO/Cu_2O surface benefited the electron transfer from CuO/Cu_2O to liquid solution with reduced energy loss. Based on the band structure match, Pb/CuO/Cu_2O catalytic membrane was able to reduce CO_2 at the Faradaic efficiency of 40.45% at -0.16 V (vs RHE). In addition, the liquid fuel generation by Pb/CuO/Cu_2O catalytic membrane was up to 0.524 μmol h^{-1} cm^{-2} for formic acid and 0.102 μmol h^{-1} cm^{-2} for methanol (Figure 19).

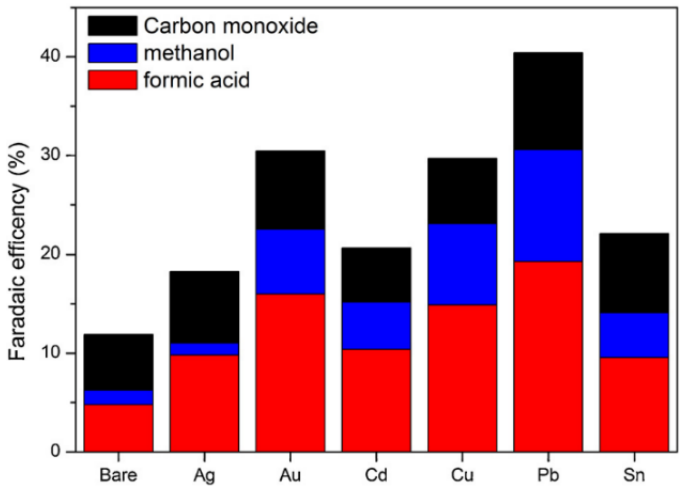

Figure 19. Faradaic efficiency of bare and metal-deposited CuO/Cu_2O photocathodes. Reproduced with permission from Ref. [95]. Copyright 2014, Elsevier.

Zhang et al. prepared a bimetallic CuZn alloy membrane for photoelectrochemical CO_2 reduction [96]. Photoelectrochemical measurements were conducted in a H-type cell under visible light irradiation. The CuZn membrane was employed as the cathode in CO_2-saturated 0.1 M $KHCO_3$ solution, while $BiVO_4$ was used as the photoanode in 0.1 M $KHCO_3$-containing 0.05 M Na_2SO_3 solution. The CuZn catalyst showed the selectivity on CO_2 reduction to HCOOH with the highest Faradaic efficiency of about 60% at 1.3 V (vs RHE) along with current density of 2.5 mA cm^{-2} (Figure 20). In the basis of experimental results and DFT calculations, the authors concluded that the presence of Zn in the CuZn catalyst was beneficial for lowering the energy barrier and stabilizing the intermediates, leading to the enhancement of HCOOH formation and suppression of HER.

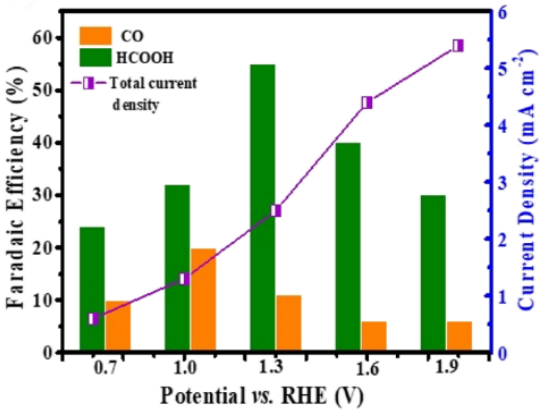

Figure 20. Faradaic efficiency ratios of the CuZn-0.5 catalyst as the cathode in CO_2-saturated 0.1 M $KHCO_3$ solution. Reproduced with permission from Ref. [96]. Copyright 2019, American Chemical Society.

3.4 Thermocatalysis for CO_2 conversion

Thermoreduction of CO_2 with catalytic membranes has been studied for about three decades, since first report by Nagara and coworkers [121]. Basically, the reduction reaction proceeds under high temperature. Gas phase CO_2 was activated by heat energy and subsequently reduced in catalytic reactor. However, the high temperature would inevitably result in high energy consumption and high production cost.

For instance, Kim et al. reported a porous nickel membrane prepared by the sintered metal method [82]. The catalytic Ni membrane was equipped in a gas-tighten assembly as shown in Figure 21 for combined steam and dry reforming to synthesize syngas. The catalytic reaction was performed with a gas feed of $(H_2O+CO_2)/CH_4$ under temperature range of 923-1023K. The authors conducted thorough studies about the influence of temperature and CO_2/H_2O feed ratio on the catalytic production. At a CO_2/H_2O ratio of 1.0, residence time of 120 ms and 1023K, a syngas production rate of 5.68×10^{-2} N m^3 h^{-1} at a H_2/CO molar ratio of

1.8 was obtained over porous Ni membrane.

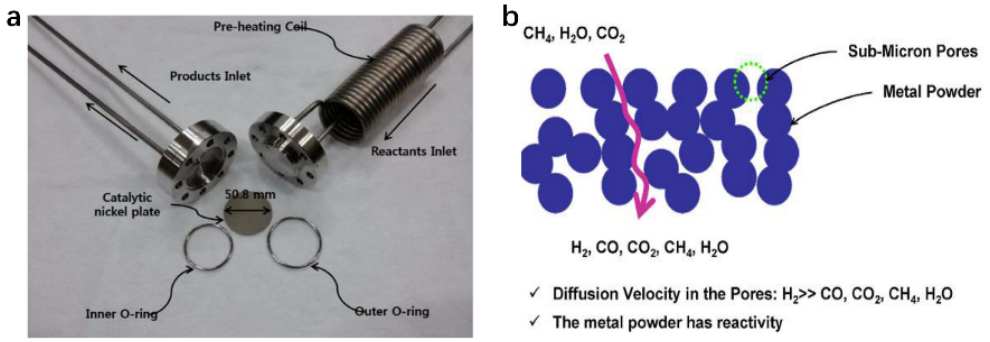

Figure 21. (a) Photograph of catalytic nickel membrane and assembly. (b) Illustration of CO_2 conversion through porous Ni membrane. Reproduced with permission from Ref. [82]. Copyright 2014, Elsevier.

3.5 Biochemical catalysis for CO_2 conversion

Enzyme-based catalysis has been developed as a promising method for CO_2 conversion. The excellent activity and selectivity of enzymes could realize CO_2 conversion under mild condition such as room temperature and normal pressure. Nevertheless, several bottleneck issues hindered its application, and the CO_2 conversion still needs a further improvement. Enzymes are often vulnerable and easy to be denaturized in extreme conditions, so that there are unique requirements for the preparation of enzyme-based catalytic membranes.

To avoid the denaturation of enzymes during the immobilization, a noncovalent bonding method, namely filtration, was utilized by Pinelo et al. to decorate three enzymes (FDH, FaldDN and ADH) onto the substrate [52]. CO_2-saturated reduced nicotinamide adenine dinucleotide solution was injected into a filtration equipment with enzyme-immobilized porous membrane. The feed solution was driven by pressure to transport through the as-prepared membrane. CO_2 was catalyzed by the enzymes into methanol during the

transmembrane transportation process, with the methanol production about 0.25 mM in the first five cycles. Based on the experiments, the authors found that FaldDH enzyme was the cascade bottleneck for CO_2 conversion to methanol.

Chen et al. prepared a biocatalytic membrane by immobilizing carbonic anhydrase (CA) onto TiO_2 film that was synthesized by a sol-gel method [53]. The CO_2 conversion test was conducted by soaking the biocatalytic membrane in Tris-HCl buffer at room temperature with CO_2 saturated water, followed by adding $CaCl_2$ in Tris buff. Dissolved CO_2 in the above solution would be hydrated and converted to $CaCO_3$ precipitate over the CA/TiO_2 membrane. The results showed that the obtained product amount over biocatalytic membrane was approximately equal to that of free CA, indicating that the immobilized CA still maintained high biocatalytic performance. Nearly 90% CO_2 in saturated solution was converted to $CaCO_3$, suggesting a high potential of biocatalytic membrane for CO_2 conversion applications.

4. Conclusions and perspectives

Catalytic CO_2 conversion to value-added chemicals offers an efficient strategy to decrease CO_2 concentration in atmosphere for mitigating the climate change. In this review, we have highlighted the motivation to convert CO_2 into chemicals and fuels and focused on porous catalytic membranes for the conversion of CO_2. Representative preparation methods for catalytic membranes have been summarized in this review. Common methods, such as electrodeposition, surface coating and filtration, have also been discussed in detail. We have reviewed various techniques for catalytic CO_2 conversion, including electocatalysis, photocatalysis, photoelectrocatalysis, thermocatalysis and biocatalysis. Recent significant

research progresses by using these techniques with catalytic membranes for CO_2 conversion have been presented.

Despite of these research progresses, the membrane-based catalytic CO_2 conversion still faces some challenges. Although numerous materials have been constructed into nanoparticles for the conversion of CO_2, only few of them have been employed for the preparation of catalytic membranes. Thus, future attention should be paid on fabricating catalytic membranes with diverse materials and porous structures. According to the property of each starting material, novel preparation methods should be put forward to obtain high quality catalytic membranes. The influence of preparation methods on catalytic performance still requires further investigations. Last but not the least, efficient CO_2 conversion devices should be built up with catalytic membranes on account of their high compatibility, since this is a critical step toward practical applications of catalytic membranes for CO_2 conversion.

Acknowledgments

The research is supported by the Ministry of Education Singapore under the Academic Research Funds (RT12/19 and MOE-MOET2EP10120-0003) and the Singapore National Research Foundation Investigatorship (NRF-NRFI2018-03).

Conflicts of interest

The authors declare that they have no known competing financial interests or personal relationships that could have appeared to influence the work reported in this paper.

References

[1] Z. Sun, N. Talreja, H. Tao, J. Texter, M. Muhler, J. Strunk, J. Chen, Angew. Chem. Int. Ed. 57 (2018) 7610-7627.

[2] C.-T. Dinh, T. Burdyny, M. G. Kibria, A. Seifitokaldani, C. M. Gabardo, F. P. García de Arquer, A. Kiani, J. P. Edwards, P. De Luna, O. S. Bushuyev, C. Zou, Science 360 (2018) 783-787.

[3] M. D. Burkart, N. Hazari, C. L. Tway, E. L. Zeitler, ACS Catal. 9 (2019) 7937-7956.

[4] C. Costentin, J.-M. Savéant, C. Tard, ACS Energy Lett. 3 (2018) 695-703.

[5] D. C. Grills, M. Z. Ertem, M. McKinnon, K. T. Ngo, J. Rochford, Coord. Chem. Rev. 374 (2018) 173-217.

[6] J. Bonin, A. Maurin, M. Robert, Coord. Chem. Rev. 344 (2017) 184-198.

[7] H. Takeda, C. Cometto, O. Ishitani, M. Robert, ACS Catal. 7 (2017) 70-88.

[8] X. Jiang, X. Nie, X. Guo, C. Song, J. G. Chen, Chem. Rev. 120 (2020) 7984-8034.

[9] D. U. Nielsen, X.-M. Hu, K. Daasbjerg, T. Skrydstrup, Nat. Catal. 1 (2018) 244-254.

[10] J. Artz, T. E. Müller, K. Thenert, J. Kleinekorte, R. Meys, A. Sternberg, A. Bardow, W. Leitner, Chem. Rev. 118 (2018) 434-504.

[11] Y. Lum, J. W. Ager, Energy Environ. Sci. 11 (2018) 2935-2944.

[12] X. Su, X.-F. Yang, Y. Huang, B. Liu, T. Zhang, Acc. Chem. Res. 53 (2019) 656-664.

[13] P. Gao, S. Dang, S. Li, X. Bu, Z. Liu, M. Qiu, C. Yang, H. Wang, L. Zhong, Y. Han, Q. Liu, W. Wei, Y. Sun, ACS Catal. 8 (2018) 571-578.

[14] T. Ouyang, H.-J. Wang, H.-H. Huang, J.-W. Wang, S. Guo, W.-J. Liu, D.-C. Zhong, T.-B. Lu, Angew. Chem. Int. Ed. 57 (2018) 16480-16485.

[15] L. Wang, Y. Yi, C. Wu, H. Guo, X. Tu, Angew. Chem. Int. Ed. 56 (2017) 13679-13683.

[16] C. Xie, C. Chen, Y. Yu, J. Su, Y. Li, G. A. Somorjai, P. Yang, Nano Lett. 17 (2017) 3798-3802.

[17] S. Zhao, N. Austin, M. Li, Y. Song, S. D. House, S. Bernhard, J. C. Yang, G. Mpourmpakis, R. Jin, ACS Catal. 8 (2018) 4996-5001.

[18] A. S. Varela, M. Kroschel, N. D. Leonard, W. Ju, J. Steinberg, A. Bagger, J. Rossmeisl, P. Strasser, ACS Energy Lett. 3 (2018) 812-817.

[19] B. M. Tackett, E. Gomez, J. G. Chen, Nat. Catal. 2 (2019) 381-386.

[20] T. K. Pal, D. De, P. K. Bharadwaj, Coord. Chem. Rev. 408 (2020) 213173.

[21] C. Gao, S. Chen, Y. Wang, J. Wang, X. Zheng, J. Zhu, L. Song, W. Zhang, Y. Xiong, Adv. Mater. 30 (2018) 1704624.

[22] G. Li, Y. Sun, Q. Zhang, Z. Gao, W. Sun, X. Zhou, Chem. Eng. J. 410 (2021) 128397.

[23] S. Mukhopadhyay, R. Shimoni, I. Liberman, R. Ifraemov, I. Rozenberg, I. Hod, Angew. Chem. Int. Ed. (2021) DOI: 10.1002/anie.202102320.

[24] L. Lin, H. Li, C. Yan, H. Li, R. Si, M. Li, J. Xiao, G.Wang, X. Bao, Adv. Mater. 31 (2019) 1903470.

[25] B. J. Hare, D. Maiti, Y. A. Daza, V. R. Bhethanabotla, J. N. Kuhn, ACS Catal. 8 (2018) 3021-3029.

[26] M. L. Ding, H. L. Jiang, ACS Catal. 8 (2018) 3194-3201.

[27] Z. Zhou, C. He, L. Yang, Y. Wang, T. Liu, C. Duan, ACS Catal. 7 (2017) 2248-2256.

[28] Q. Li, J. Fu, W. Zhu, Z. Chen, B. Shen, L. Wu, Z. Xi, T. Wang, G. Lu, J.-j. Zhu, S. Sun, J. Am. Chem. Soc. 139 (2017) 4290-4293.

[29] J. Qin, S. Wang, X. Wang, Appl. Catal. B 209 (2017) 476-482.

[30] A. Fujishima, K. Honda, Nature 238 (1972) 37-38.

[31] H.-R. M. Jhong, C. E. Tornow, B. Smid, A. A. Gewirth, S. M. Lyth, P. J. A. Kenis, ChemSusChem 10 (2017) 1094-1099.

[32] J. He, N. J. J. Johnson, A. Huang, C. P. Berlinguette, ChemSusChem 11 (2018) 48-57.

[33] J. Fu, W. Zhu, Y. Chen, Z. Yin, Y. Li, J. Liu, H. Zhang, J.-J.Zhu, S. Sun, Angew. Chem. Int. Ed. 58 (2019) 14100-14103.

[34] F. Li, Y. C. Li, Z. Wang, J. Li, D.-H. Nam, Y. Lum, M. Luo, X. Wang, A. Ozden, S.-F. Hung, B. Chen, Y. Wang, J. Wicks, Y. Xu, Y. Li, C. M. Gabardo, C.-T. Dinh, Y. Wang, T.-T. Zhuang, D. Sinton, E. H. Sargent, Nat. Catal. 3 (2020) 75-82.

[35] J. H. Koh, D. H. Won, T. Eom, N.-K. Kim, K. D. Jung, H. Kim, Y. J. Hwang, B. K. Min, ACS Catal. 7 (2017) 5071-5077.

[36] X. J. Bai, X. Y. Lu, R. Ju, H. Chen, L. Shao, X. Zhai, Y. N. Li, F. Q. Fan, Y. Fu, W. Qi, Angew. Chem. Int. Ed. 60 (2021) 701-705.

[37] X. Lin, Y. Gao, M. Jiang, Y. Zhang, Y. Hou, W. Dai, S. Wang, Z. Ding, Appl. Catal. B 224 (2018) 1009-1016.

[38] H. Seo, A. Liu, T. F. Jamison, J. Am. Chem. Soc. 139 (2017) 13969-13972.

[39] L. Ye, Y. Gao, S. Cao, H. Chen, Y. Yao, J. Hou, L. Sun, Appl. Catal. B 227 (2018) 54-60.

[40] M. Zhou, S. Wang, P. Yang, Z. Luo, R. Yuan, A. M. Asiri, M. Wakeel, X. Wang, Chem. Eur. J. 24 (2018) 18529-18534.

[41] J. Zhao, B. Liu, L. Meng, S. He, R. Yuan, Y. Hou, Z. Ding, H. Lin, Z. Zhang, X. Wang, J. Long, Appl. Catal. B 256 (2019) 117823.

[42] Y. Bai, P. Yang, L. Wang, B. Yang, H. Xie, Y. Zhou, L. Ye, Chem. Eng. J. 360 (2019) 473-482.

[43] M. Zhou, S. Wang, P. Yang, C. Huang, X. Wang, ACS Catal. 8 (2018) 4928-4936.

[44] J. T. Song, H. Ryoo, M. Cho, J. Kim, J. G. Kim, S. Y. Chung, J. Oh, Adv. Energy Mater. 7 (2017) 201601103.

[45] J. K. Sheu, P. H. Liao, Y. C. Lee, H. K. Wang, M. L. Lee, J. Phys. Chem. C 124 (2020) 9591-9598.

[46] P. T. S. de la Cruz, K. Irikura, A. Lachgar, J. C. Cardoso, H. A. Cavero, M. V. B. Zanoni, Electrocatalysis 11 (2020) 546-554.

[47] H. Büttner, J.Steinbauer, C. Wulf, M. Dindaroglu, H.-G. Schmalz, T. Werner, ChemSusChem 10 (2017) 1076-1079.

[48] A. Ramirez, A. Dutta Chowdhury, A. Dokania, P. Cnudde, M. Caglayan, I. Yarulina, E. Abou-Hamad, L. Gevers, S. Ould-Chikh, K. De Wispelaere, V. van Speybroeck, J. Gascon, ACS Catal. 9 (2019) 6320-6334.

[49] B. An, Z. Li, Y. Song, J. Zhang, L. Zeng, C. Wang, W. Lin, Nat. Catal. 2 (2019) 709-717.

[50] Z. Li, Y. Qu, J. Wang, H. Liu, M. Li, S. Miao, C. Li, Joule 3 (2019) 570-583.

[51] A. Ramirez, L. Gevers, A. Bavykina, S. Ould-Chikh, J. Gascon, ACS Catal. 8 (2018) 9174-9182.

[52] J. Luo, A. S. Meyer, R. V. Mateiu, M. Pinelo, New Biotechnol. 32 (2015) 319-327.

[53] J. W. Hou, G. X. Dong, B. W. Xiao, C. Malassigne, V. Chen, J. Mater. Chem. A 3 (2015) 3332-3342.

[54] K. A. Grice, Coord. Chem. Rev. 336 (2017) 78-95.

[55] H. Rao, C.-H. Lim, J. Bonin, G. M. Miyake, M. Robert, J. Am. Chem. Soc. 140 (2018) 17830-17834.

[56] C. Cometto, L. Chen, P.-K. Lo, Z. Guo, K.-C. Lau, ACS Catal. 8 (2018) 3411-3417.

[57] A. Chapovetsky, M. Welborn, J. M. Luna, R. Haiges, T. F. Miller, S. C. Marinescu, ACS Cent. Sci. 4 (2018) 397-404.

[58] S. Ren, D. Joulié, D. Salvatore, K. Torbensen, M. Wang, M. Robert, C. P. Berlinguette, Science 365 (2019) 367-369.

[59] S. Zhang, Q. Fan, R. Xia, T. J. Meyer, Acc. Chem. Res. 53 (2020) 255-264.

[60] N. Wei, Y. Zhang, L. Liu, Z.-B. Han, D.-Q. Yuan, Appl. Catal. B 219 (2017) 603-610.

[61] B. Han, X. Ou, Z. Deng, Y. Song, C. Tian, H. Deng, Y.-J. Xu, Z. Lin, Angew. Chem. Int. Ed. 57 (2018) 16811-16815.

[62] J. Di, C. Zhu, M. Ji, M. Duan, R. Long, C. Yan, K. Gu, J. Xiong, Y. She, J. Xia, H. Li, Z. Liu, Angew. Chem. Int. Ed. 57 (2018) 14847-14851.

[63] S. Das, J. Pérez-Ramírez, J. Gong, N. Dewangan, K. Hidajat, B. C. Gates, S. Kawi, Chem. Soc. Rev. 49 (2020) 2937-3004.

[64] S. Nellaiappan, N. K. Katiyar, R. Kumar, A. Parui, K. D. Malviya, K. G. Pradeep, A. K. Singh, S. Sharma, C. S. Tiwary, K. Biswas, ACS Catal. 10 (2020) 3658-3663.

[65] B. Kumar, V. Atla, J. P. Brian, S. Kumari, T. Q. Nguyen, M. Sunkara, J. M. Spurgeon, Angew. Chem. Int. Ed. 56 (2017) 3645-3649.

[66] S. Yang, W. Hu, X. Zhang, P. He, B. Pattengale, C. Liu, M. Cendejas, I. Hermans, X.Zhang, J. Zhang, J. Huang, J. Am. Chem. Soc. 140 (2018) 14614-14618.

[67] Y. Wang, J.Liu, Y. Wang, A. M. Al-Enizi, G. Zheng, Small 13 (2017) 1701809.

[68] S. N. Talapaneni, G.Singh, I. Y. Kim, K. AlBahily, A. a. H. Al-Muhtaseb, A. S. Karakoti, E. Tavakkoli, A. Vinu, Adv. Mater. 32 (2020) 1904635.

[69] R. Luo, Y. Chen, Q. He, X. Lin, Q. Xu, X. He, W. Zhang, X. Zhou, H. Ji, ChemSusChem 10 (2017) 1526-1533.

[70] Z. Sun, T. Ma, H. Tao, Q. Fan, B. Han, Chem 3 (2017) 560-587.

[71] T. Zheng, K. Jiang, H. Wang, Adv. Mater. 30 (2018) 1802066.

[72] E. Bertin, S. Garbarino, C. Roy, S. Kazemi, D. Guay, J. CO_2 Util. 19 (2017) 276-283.

[73] J. Rosen, G. S. Hutchings, Q. Lu, R. V. Forest, A. Moore, F. Jiao, ACS Catal. 5 (2015) 4586-4591.

[74] J. Y. Kim, C. H. Ryu, J. H. Lee, A. U. Pawar, W. D. Jang, Y. S. Kang, H. S. Ahn, ACS Appl. Energy Mater. 3 (2020) 6670-6677.

[75] M. Ma, K. Liu, J. Shen, R. Kas, W. A. Smith, ACS Energy Lett. 3 (2018) 1301-1306.

[76] P. L. Cheung, S. K. Lee, C. P. Kubiak, Chem. Mater. 31 (2019) 1908-1919.

[77] A. R. Paris, A. B. Bocarsly, ACS Catal. 9 (2019) 2324-2333.

[78] G. K. Ramesha, J. F. Brennecke, P. V. Kamat, ACS Catal. 4 (2014) 3249-3254.

[79] W. A. Thompson, C. Perier, M. M. Maroto-Valer, Appl. Catal. B 238 (2018) 136-146.

[80] Y. H. Hou, S. Bolat, A. Bornet, Y. E. Romanyuk, H. Z.Guo, P. Moreno-Garcia, I. Z. Montiel, Z. Q. Lai, U. Muller, V. Grozovski, P. Broekrnann, ACS Catal. 9 (2019) 9518-9529.

[81] Y. Guo, B. Gao, Z. Deng, Y. Liu, X. Peng, Y. Zhao, J. Mater. Chem. A 9 (2021) 2694-2699.

[82] S. K. Ryi, S. W. Lee, J. W. Park, D. K. Oh, J. S. Park, S. S. Kim, Catal. Today 236 (2014) 49-56.

[83] Y. T. Guntern, J. R. Pankhurst, J. Vvra, M. Mensi, V. Mantella, P. Schouwink, R. Buonsanti, Angew. Chem. Int. Ed. 58 (2019) 12632-12639.

[84] H. P. Yang, Y. Wu, G. D. Li, Q. Lin, Q. Hu, Q. L. Zhang, J. H. Liu, C. He, J. Am. Chem. Soc. 141 (2019) 12717-12723.

[85] T. T. H. Hoang, S. C. Ma, J. I. Gold, P. J. A. Kenis, A. A. Gewirth, ACS Catal. 7 (2017) 3313-3321.

[86] C. W. Kung, C. O. Audu, A. W. Peters, H. Noh, O. K. Farha, J. T. Hupp, ACS Energy Lett. 2 (2017) 2394-2401.

[87] X. Y. Zhang, B. M. Huang, C. H. Sun, W. Lu, Z. Q. Tian, P. K. Shen, H. T. Wang, D. Y. Zhao, D. R. Macfarlane, ACS Energy Lett. 3 (2018) 2649-2655.

[88] M. Ma, K. Djanashvili, W. A. Smith, Angew. Chem. Int. Ed. 55 (2016) 6680-6684.

[89] H. Coskun, A. Aljabour, P. De Luna, D. Farka, T. Greunz, D. Stifter, M. Kus, X. L. Zheng, M. Liu, A. W. Hassel, W. Schofberger, E. H. Sargent, N. S. Sariciftci, P. Stadler, Sci. Adv. 3 (2017) 1700686.

[90] J. Li, G. X. Chen, Y. Y. Zhu, Z. Liang, A. Pei, C. L. Wu, H. X. Wang, H. R. Lee, K. Liu, S. Chu, Y. Cui, Nat. Catal. 1 (2018) 592-600.

[91] J. W. Maina, C. Pozo-Gonzalo, J. A. Schutz, J. T. Wang, L. F. Dumee, Carbon 148 (2019) 80-90.

[92] A. Brunetti, F. R. Pomilla, G. Marci, E. I. Garcia-Lopez, E. Fontananova, L. Palmisano, G. Barbieri, Appl. Catal. B 255 (2019) 117779.

[93] J. W. Maina, J. A. Schutz, L. Grundy, E. D. Ligneris, Z. F. Yi, L. X. Kong, C. Pozo-Gonzalo, M. Ionescu, L. F. Dumee, ACS Appl. Mater. Interfaces 9 (2017) 35010-35017.

[94] L. Wang, D. W. Bahnemann, L. Bian, G. H. Dong, J. Zhao, C. Y. Wang, Angew. Chem. Int. Ed. 58 (2019) 8103-8108.

[95] D. H. Won, C. H. Choi, J. Chung, S. I. Woo, Appl. Catal. B 158 (2014) 217-223.

[96] S. Ajmal, Y. Yang, K. J. Li, M. A. Tahir, Y. Y. Liu, T. Wang, A. U. R. Bacha, Y. Q. Feng, Y. Deng, L. W. Zhang, J. Phys. Chem. C 123 (2019) 11555-11563.

[97] J. M. Barlow, J. Y. Yang, ACS Cent. Sci. 5 (2019) 580-588.

[98] X. Tan, C. Yu, Y. Ren, S. Cui, W. Li, J. Qiu, Energy Environ. Sci. 14 (2021) 765-780.

[99] J. Zeng, K. Bejtka, W. Ju, M. Castellino, A. Chiodoni, A. Sacco, M. A. Farkhondehfal, S. Hernández, D. Rentsch, C. Battaglia, C. F. Pirri, Appl. Catal. B 236 (2018) 475-482.

[100] L. Yuan, S.-F. Hung, Z.-R. Tang, H. M. Chen, Y. Xiong, Y.-J. Xu, ACS Catal. 9 (2019) 4824-4833.

[101] B. Wang, J. Di, L. Lu, S. Yan, G. Liu, Y. Ye, H. Li, W. Zhu, H. Li, J. Xia, Appl. Catal. B 254 (2019) 551-559.

[102] Y. Bai, L. Ye, T. Chen, P. Wang, L. Wang, X. Shi, P. K. Wong, Appl. Catal. B 203 (2017) 633-640.

[103] P. Yang, H. Zhuzhang, R. Wang, W. Lin, X. Wang, Angew. Chem. Int. Ed. 58 (2019) 1134-1137.

[104] G. Zhang, G. Li, T. Heil, S. Zafeiratos, F. Lai, A. Savateev, Antonietti, X. Wang, Angew. Chem. Int. Ed. 58 (2019) 3433-3437.

[105] L. Hao, L. Kang, H. Huang, L. Ye, K. Han, S. Yang, H. Yu, M. Batmunkh, Y. Zhang, T. Ma, Adv. Mater. 31 (2019) 1900546.

[106] J. Shan, F. Raziq, M. Humayun, W. Zhou, Y. Qu, G. Wang, Y. Li, Appl. Catal. B 219

(2017) 10-17.

[107] J. Wang, C. Qin, H. Wang, M. Chu, A. Zada, X. Zhang, J. Li, F. Raziq, Y. Qu, L. Jing, Appl. Catal. B 221 (2018) 459-466.

[108] X. Wu, Y. Li, G. Zhang, H. Chen, J. Li, K. Wang, Y. Pan, Y. Zhao, Y. Sun, Y. Xie, J. Am. Chem. Soc. 141 (2019) 5267-5274.

[109] Q. Han, X. Bai, Z. Man, H. He, L. Li, J. Hu, A. Alsaedi, T. Hayat, Z. Yu, W. Zhang, J. Wang, Y. Zhou, Z. Zou, J. Am. Chem. Soc. 141 (2019) 4209-4213.

[110] K. M. Choi, D. Kim, B. Rungtaweevoranit, C. A. Trickett, J. T. D. Barmanbek, A. S. Alshammari, P. Yang, O. M. Yaghi, J. Am. Chem. Soc. 139 (2017) 356-362.

[111] S. Liu, F. Chen, S. Li, X. Peng, Y. Xiong, Appl. Catal. B 211 (2017) 1-10.

[112] F. Raziq, Y. Qu, M. Humayun, A. Zada, H. Yu, L. Jing, Appl. Catal. B 201 (2017) 486-494.

[113] C. Kim, K. M. Cho, A. Al-Saggaf, I. Gereige, H.-T. Jung, ACS Catal. 8 (2018) 4170-4177.

[114] J. Bian, J. Feng, Z. Zhang, Z. Li, Y. Zhang, Y. Liu, S. Ali, Y. Qu, L. Bai, J. Xie, D. Tang, X. Li, F. Bai, J. Tang, L. Jing, Angew. Chem. Int. Ed. 58 (2019) 10873-10878.

[115] G. Zhang, H. Yang, H. Fei, ACS Catal. 8 (2018) 2519-2525.

[116] H. H. Wang, L. Hou, Y. Z. Li, C. Y. Jiang, Y. Y. Wang, Z. H. Zhu, ACS Appl. Mater. Interfaces 9 (2017) 17969-17976.

[117] M. Taherimehr, B. VandeVoorde, L. H. Wee, J. A. Martens, D. E. DeVos, P. P. Pescarmona, ChemSusChem 10 (2017) 1283-1291.

[118] S.-L. Hou, J. Dong, X.-L. Jiang, Z.-H. Jiao, B. Zhao, Angew. Chem. Int. Ed. 58 (2019)

577-581.

[119] S. Xu, E. A. Carter, Chem. Rev. 119 (2019) 6631-6669.

[120] A. U.m Pawar, C. W. Kim, M.-T. Nguyen-Le, Y. S. Kang, ACS Sustain. Chem. Eng. 7 (2019) 7431-7455.

[121] N. Yutaka, C. Bernard, Bull. Chem. Soc. Jpn. 59 (1986) 1997-2002.

Graphical Abstract

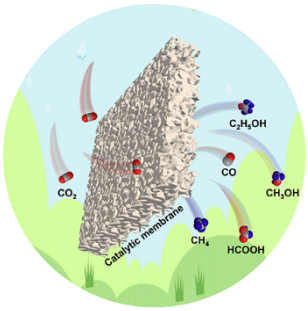

Porous catalytic membranes are promising systems for converting CO_2 into value-added chemicals. Recent research progress in the preparations of porous catalytic membranes for CO_2 conversion is reviewed.